1-1-2018

Activating Titania for Efficient Electrocatalysis by Vacancy Engineering

Haifeng Feng
University of Wollongong, Beihang University, hf533@uowmail.edu.au

Zhongfei Xu
Beihang University, xuzfei@buaa.edu.cn

Long Ren
University of Wollongong, lr289@uowmail.edu.au

Chen Liu
Chinese Academy of Sciences, cl565@uowmail.edu.au

Jincheng Zhuang
University of Wollongong, jincheng@uow.edu.au

See next page for additional authors

Recommended Citation

Activating Titania for Efficient Electrocatalysis by Vacancy Engineering

Abstract

Pursuing efficient and low-cost electrocatalysts is crucial for the performance of water-alkali electrolyzers toward water splitting. Earth-abundant transition-metal oxides, in spite of their alluring performances in the oxygen evolution reaction, are thought to be inactive in the hydrogen evolution reaction in alkaline media. Here, we demonstrate that pure TiO_2 single crystals, a typical transition-metal oxide, can be activated toward electrocatalytic hydrogen evolution reaction in alkaline media through engineering interfacial oxygen vacancies. Experimental and theoretical results indicate that subsurface oxygen vacancies and low-coordinated Ti ions (Ti^{3+}) can enhance the electrical conductivity and promote electron transfer and hydrogen desorption, which activate reduced TiO_2 single crystals in the hydrogen evolution reaction in alkaline media. This study offers a rational route for developing reduced transition-metal oxides for low-cost and highly active hydrogen evolution reaction catalysts, to realize overall water splitting in alkaline media.

Disciplines

Engineering | Physical Sciences and Mathematics

Publication Details

Authors

Haifeng Feng, Zhongfei Xu, Long Ren, Chen Liu, Jincheng Zhuang, Zhenpeng Hu, Xun Xu, Jun Chen, Jiaou Wang, Weichang Hao, Yi Du, and Shi Xue Dou

Activating Titania for Efficient Electrocatalysis by Vacancy Engineering

Haifeng Feng,[†,§,⊥] Zhongfei Xu,[‡,§,⊥] Long Ren,[†,⊥] Chen Liu,[∥] Jincheng Zhuang,[†] Zhenpeng Hu,[#,*] Xun Xu,[†,§] Jun Chen,[∇] Jiaou Wang,[∥] Weichang Hao,[‡,§,*] Yi Du,[†,§,*] and Shi Xue Dou,[†,§]

[†]Institute for Superconducting and Electronic Materials, Australian Institute for Innovative Materials, University of Wollongong, Wollongong, NSW 2500, Australia

[‡]Department of Physics and Key Laboratory of Micro-Nano Measurement, Manipulation and Physics, Ministry of Education, Beihang University, Beijing 100191, P. R. China

[§]Beihang-UOW Joint Research Centre, Beihang University, Beijing 100191, P. R. China

[∥]Beijing Synchrotron Radiation Facility, Institute of High Energy Physics, Chinese Academy of Sciences, Beijing 100049, P. R. China

[#]School of Physics, Nankai University, Tianjin 300071, P. R. China

[∇]Intelligent Polymer Research Institute and ARC Centre of Excellence for Electromaterials Science, University of Wollongong, Wollongong, NSW 2500, Australia

ABSTRACT: Pursuing efficient and low-cost electrocatalysts is crucial for the performance of water-alkali electrolyzers towards water splitting. Earth-abundant transition metal oxides, in spite of their alluring performances in the oxygen evolution reaction, are thought to be inactive in the hydrogen evolution reaction in alkaline media. Here, we demonstrate that pure TiO_2 single crystal, a typical transition metal oxide, can be activated towards electrocatalytic hydrogen evolution reaction in alkaline media through engineering interfacial oxygen vacancies. Experimental and theoretical results indicate that subsurface oxygen vacancies and low coordinated Ti ions (Ti^{3+}) can enhance the electrical conductivity and promote electron transfer and hydro-gen desorption, which activate reduced TiO_2 single crystal in the hydrogen evolution reaction in alkaline media. This study offers a rational route for developing reduced transition metal oxide for low-cost and highly active hydrogen evolution reaction catalysts, to realize over all water splitting in alkaline media.

KEYWORDS: Titania, oxygen vacancy, hydrogen evolution reaction, alkaline media, Ti^{3+} ions, water splitting, in-situ STM observation

Introduction

Water-alkali electrolyzers for overall water splitting exhibit tremendous potential for the evolution of high-purity hydrogen and oxygen gases, with the additional values of simple processes, zero CO_2 emissions, and low pollutants.[1] Pursuing efficient, low-cost, and non-precious-metal electrocatalysts for the hydrogen evolution reaction (HER) or the oxygen evolution reaction (OER), or both, is the central research interest in recent progress towards large-scale industrialization. A variety of highly-active earth-abundant transition metal oxides (TMOs) have been proven to be appealing alternatives to noble-metal based (Ir, Ru, Pt)

electrocatalysts for the OER in alkaline media. Their success has stimulated research interest in exploring TMOs as electrocatalysts for the HER in alkaline media,[2-8] which can realize overall water splitting by electrocatalysis in a cheap, feasible, and durable way to create clean energy. Unfortunately, most TMOs exhibit intrinsically low electrical conductivity and unfavorable hydrogen adsorption desorption capability, which hinders their use as electrocatalysts for the HER in alkaline media.[8-10]

In order to overcome these obstacles, great efforts have been dedicated to the development of complex TMO systems for the HER in alkaline media, which include transition metal (TM)/TMO/carbon hierarchical structures,[11-15] mixed TMOs,[16-20] and reduced or metallic TMOs[21-26]. In these TMO-based electrocatalysts, conductive supporting materials, such as carbon nanofibers, carbon nanotubes, and Ni foam, can effectively increase the electrical conductivity of the TMOs. This enables effective charge transfer in the electrocatalytic process to occur on the surfaces of electrocatalysts. The TMO components can promote water dissociation to produce hydrogen intermediates (H_{ads}).[9,15,21] The H_{ads} adsorbed on the active sites on metals with low coordination numbers (such as Ni and Co) could recombine into hydrogen molecules.[11,23] Despite considerable progress in the preparation of TMO-based electrocatalysts for the HER in alkaline media, it still remains a challenge to precisely synthesize these composite electrocatalysts with controllable structures and reproducible performances, due to their complicated preparation and complex structures. Alternatively, given their excellent water dissociation capability, simple-component TMOs are expected to be used in electrocatalysis for the HER in alkaline media if their low electrical conductivity and unfavorable H_{ads} adsorption/desorption capability could be overcome.[27-29]

Herein, we demonstrate that rutile TiO_2 single crystal can be activated towards the HER in alkaline media by thermal reduction in vacuum conditions. It shows unexpected HER activity with excellent stability and durability in alkaline media. Oxygen vacancies (OVs) and low-coordinated Ti ions (Ti^{3+}) dominate the HER activity of the reduced TiO_2 single crystal by modulating the electrical conductivity and facilitating charge transfer among electrocatalytic active sites and H_{ads}. Combined with density functional theory (DFT) calculations on the Gibbs free energy, the overall pathways of the electrocatalytic HER over reduced TiO_2 in alkaline media are revealed. This work provides a fundamental understanding of the electrocatalytic activity of thermally reduced TiO_2 towards the HER, which is of immense scientific importance towards the development of high-performance, low-cost, and durable TMOs-based electrocatalysts for overall water splitting in alkaline media.

Result

Reduced $TiO_2(110)$ samples were prepared through annealing stoichiometric $TiO_2(110)$ single crystals in ultra-high vacuum (UHV, $< 1 \times 10^{-10}$ Torr) at 900 K. The highly crystalline structure of the reduced TiO_2 single crystal has been verified by cross-sectional high-angle annular dark-field (HAADF) images, as shown in Fig. 1a. The corresponding crystal structure is illustrated in the Fig. 1a inset, in which the rows of bridging oxygen (O_{br}) atoms and five-coordinated titanium (Ti_{5C}) atoms alternately lie in a plane along the [001] direction.[30] Fig. 1b shows a large scale HAADF image of the reduced TiO_2 single crystal, in which gradually darkening contrast is observed from the bulk region (with a depth of 100 nm) to the top surface, suggesting that the oxygen deficiency (or OVs) increases from the bulk region to the surface, as the contrast in HAADF mode is proportional to the average atomic number of atomic columns.[31] The removed oxygen atoms leave behind two excess electrons per OV, which will be harvested by the

neighboring Ti atoms and induce the formation of Ti^{3+} ions near the surface region. This was confirmed by Ti $2p$ X-ray photoelectron spectroscopy (XPS) spectra collected from the reduced TiO_2 single crystal (Fig. 1e). A peak assigned to Ti^{3+} ions was observed around 457 eV. The oxygen deficiency distribution in the reduced TiO_2 single crystal was analyzed by in-situ electron energy loss spectroscopy (EELS). The core-level and Ti-L edge spectra were acquired at three different regions (10 nm, 50 nm, and 100 nm below the surface), which are marked in Fig. 1b. As shown in the Ti-L edge spectra (Fig. 1c), the gradual reduction of the t_{2g}/e_g peak area ratio along with the less resolved e_g splitting ($\Delta = d_{z2} - d_{x2-y2}$) at the Ti-$L3$ edge in reduced TiO_2 is clearly shown from the bulk region to the surface. This reflects the presence of Ti^{3+} ions and their gradually increasing concentration from the bulk region to the surface. Since the Ti^{3+} ions are given rise to the OVs, a gradually increasing concentration of OVs from the bulk region to the surface in reduced TiO_2 single crystal can be revealed and has been plotted in Fig. 1d (See more STEM and EELS results in Figs. S1-S4 in Supporting Information). In XPS valence band spectra (Fig. 1e inset), an additional mid-gap state (generally denoted as the Ti $3d$ defect state) located at 0.8 eV below the Fermi level was observed, which is attributed to the OVs in the surface area (see DFT calculations of the mid-gap states caused by OVs in Fig. S5 in Supporting Information).

To evaluate the electrocatalytic activity of reduced TiO_2 single crystals, two TiO_2 samples with different OV concentrations (OV-low TiO_2 and OV-high TiO_2 single crystals) were selected to assess their HER performance in alkaline media. The OV-low TiO_2 and OV-high TiO_2 single crystals were annealed at 900 K in UHV for 5 hours and 50 hours, respectively. A Nb-doped (0.43 at%) TiO_2 single crystal was also selected as a reference sample to perform HER under the same conditions. As shown in Fig. 2a, OV-high TiO_2 exhibited considerable HER activity with a

current density of 22.8 mA.cm^{-2} at −0.80 V in 1 M KOH aqueous solution. It showed excellent HER stability in alkaline media, which was verified by a cycling test of 1000 consecutive cycles (Fig. 2a), and superior durability in HER activity over 18 hours of continuous operation at −0.7 V versus reversible hydrogen electrode (RHE) (Fig. 2b). The chemical stability of OV-high TiO$_2$ was also confirmed by the unchanged Raman spectra obtained before and after the cycling test in Fig. S6 in Supporting Information. The Tafel slope near the substantial cathodic current region is 187.5 mV·dec^{-1}, as plotted in Fig. 2c. In contrast, the OV-low TiO$_2$ was not electrocatalytically active under the same conditions, while the reference Nb-doped TiO$_2$ single crystal exhibited very weak electrocatalytic HER activity. As is well known, electrical conductivity and the number of electrocatalytic sites are of great significance for the catalytic performance of electrocatalysts. Five-probe Hall effect measurements (Figs. S7 and S8 in Supporting Information) were carried out to reveal the conductivities of all the TiO$_2$ single crystals. It was found that the OV-high TiO$_2$ showed electrical resistivity of 80.0 × 10^{-3} Ω·m, which is lower than that of the OV-low TiO$_2$ (94.0 × 10^{-3} Ω·m). The charge carrier density in OV-high TiO$_2$ (1.9 × 10^{17} cm^{-3}) is about 40 times higher than that in the OV-low TiO$_2$ (4.8 × 10^{15} cm^{-3}). The conductivities of both reduced TiO$_2$ samples are believed to arise from the mid-gap state induced by OVs (Fig. 1e). The reference Nb-doped TiO$_2$ single crystal exhibits the highest electrical conductivity of 40.6 × 10^{-3} Ω·m and the highest charge carrier density of 3.2 × 10^{17} cm^{-3} among all the samples. The weak electrocatalytic activity of the reference Nb-doped TiO$_2$ single crystal, however, demonstrates that good electrical conductivity is inadequate to enable TiO$_2$ activity towards the HER in alkaline media. Fig. 2d shows the double layer capacitance (C$_{dl}$) values of the three samples, which were obtained by fitting the slope of the capacitive current versus scan rate measured from the cyclic voltammetry (CV) curves (Fig. S10 in Supporting Information).

The OV-high TiO_2 shows the C_{dl} value of 72.4 mF.cm^{-2}, which is much higher than for the OV-low TiO_2 (C_{dl} = 16.0 mF.cm^{-2}) and the reference Nb-doped TiO_2 (C_{dl} = 8.8 mF.cm^{-2}). Because the C_{dl} is proportional to the electrochemically active surface area (EASA) of catalysts, this suggests that the elevated electrochemical HER of OV-high TiO_2 is not only given rise by the increased electrical conductivity and the charge carrier density, but also attributed to the large number of electrocatalytically active sites.

In order to reveal the catalytic process associated with active sites at the atomic level, scanning tunneling microscopy (STM) investigations were carried out on the OV-high TiO_2(110) single crystal. Terraces with a width of several hundred nanometers and a 1 × 1 structure can be identified in the OV-high TiO_2(110) surface, as shown in Figs. S11 and S12 in Supporting Information. Three bright protrusions were observed, which represent OV point defects, adsorbed H_2O molecules (Ad-H_2O), and OH groups. Their apparent heights allow us to identify them in STM images (see detailed descriptions in Figs. S13 and S14 in Supporting Information). It should be noted that OVs are the majority structural defects on the surface of the OV-high TiO_2(110) single crystal. All the adsorbed H_2O molecules reside on OV sites, which has been confirmed by the adsorption dynamics observed in STM (Fig. 3a and 3b). OHs also appeared on the OV sites after dissociation of H_2O molecules (Fig. S15 in Supporting Information). This phenomenon suggests that surface OVs are highly active towards adsorbing and dissociating residual H_2O molecules in UHV. In addition, each OV induces two surrounding Ti^{3+} ions, which was revealed in STM images taken with negative sample bias (filled-state), as shown in Fig. 3c and 3d. Recent investigations pointed out that the Ti^{3+} ions in reduced TiO_2 exhibit polaron behavior.[32-34] This enables Ti^{3+} ions to rapidly hop across the nearby lattice in rutile, and thus, leads to the reduced rutile TiO_2 conductivity. Since the electrical conductivity of reduced TiO_2 is

proportional to the concentration of Ti^{3+} ions, this supports the proposition that the OV-high TiO$_2$(110) single crystal possesses higher conductivity than the OV-low sample. In order to simulate electrocatalytic HER processes, we applied a sample bias to allow the STM tip to act as an electron donor to the OV-high TiO$_2$(110) single crystal surface.[35,36] Both Ad-H$_2$O and OHs disappeared from the sample surface when the bias was higher than the threshold of 2.0 V, as shown in Fig. 3e and 3f. Meanwhile, the OVs at corresponding sites were also healed. This indicates that hydrogen desorption of Ad-H$_2$O and OHs occurred on the OV-high TiO$_2$(110) surface at the cost of consumption of OVs. In this case, the HER activity of reduced TiO$_2$(110) single crystal is expected to be depressed gradually with a decreasing concentration of OVs. Nevertheless, this contradicts our cycling stability results in Fig. 2a and 2b, in which the OV-high TiO$_2$(110) surface exhibited excellent stability and durability, suggesting that OVs in the surface are not adequate to drive the electrocatalytic HER constantly and steadily, although they are active towards adsorbing H$_2$O molecules and OHs.

The origins of the electrocatalytic HER activity of the reduced TiO$_2$(110) surface in alkaline media was further revealed by DFT calculations, in terms of thermodynamics and kinetics, as shown in Fig. 4. The surface structures were modeled according to STEM and STM results obtained on TiO$_2$(110) surface with OVs. As shown in Fig. 4a, it was found that water molecules prefer to be dissociated at surface OV (surfOV) site in initial stage (step 1). The produced hydrogen atoms are favorable towards combing in pairs and forming hydrogen molecules (step 2 to 3 in Fig. 4a). All the reaction steps are exothermic processes. This supports our hypothesis that the surface OVs are easily to be healed during the electrochemical reaction. Hence, it indicates that surfOVs were not sustainable which agrees with STM observations in Fig. 3. HER pathway on the reduced TiO$_2$ with sublayer OV (subOV), as well as the pristine TiO$_2$ were further

calculated, as shown in Fig. 4b (see the main reaction pathway and overall pathway in Fig. S17 and S18 in Supporting Information, respectively). Hydrogen desorption reaction (Heyrovsky reaction) step between intermediate 2 and intermediate 3 is determined to be the rate-limiting step with the largest free energy difference for both pristine TiO_2 and reduced TiO_2. The pristine TiO_2 needs a theoretical potential of $U_{RHE} = -1.33$ eV to overcome this energy barrier. In contrast, the potential barrier can be effectively lowered on the reduced TiO_2 to enable all HER reaction steps to be exothermic and energetically favorable, due to the presence of subOV. This has been confirmed experimentally in our electrocatalytic HER process, in which onset potential for HER in reduced TiO_2 was significantly decreased. Therefore, the theoretical calculations suggest that the electrocatalytic HER activity of reduced $TiO_2(110)$ single crystal mainly originates from subOVs, which can effectively promote the hydrogen desorption capability and lower the overpotential of HER in alkaline media.

Discussion

Our study shows that inactive pure rutile $TiO_2(110)$ single crystal can be activated towards the HER in alkaline media through creating OVs and accompanying Ti^{3+} ions by annealing in UHV. OVs and Ti^{3+} ions in the surface region dominate the electrical conductivity of reduced TiO_2 and the amount of electrocatalytic active sites. Combining the well-characterized atomic surface structure and theoretical calculations, we conclude that subOVs can promote the electron transfer and hydrogen desorption in the electrocatalytic HER on reduced TiO_2 in alkaline media. Considering that all the electrochemical characterizations were performed on a single crystal sample with atomically flat surface and low specific surface area, the overpotential is expected to be significantly decreased in reduced TiO_2 nanoparticles with a higher density of active sites. In addition, the rich diversity of defects, facets, polymorphs and morphologies of TiO_2, which have

great impacts on its electrocatalytic activities, allow its electrocatalytic activities to be further enhanced through rational engineering and optimization. Our work helps to elucidate the fundamental mechanism of the electrocatalytic activity of reduced oxides towards the HER, which is of immense fundamental and practical importance towards an in-depth understanding and rational optimization of TMOs as electrocatalysts in alkaline media.

ASSOCIATED CONTENT

Supporting Information. This material is available free of charge via the Internet at http://pubs.acs.org.

Materials and Methods, Figs. S1 to S18 and Table S1.

AUTHOR INFORMATION

Corresponding Author

* yi_du@uow.edu.au

* whao@buaa.edu.cn

* zphu@nankai.edu.cn

Author Contributions

⊥These authors contributed equally.

H.F, W.H and Y.D designed the experiments; H.F and J.Z conducted synthesis; Z.X, Z.H and W.H conducted computational modelling and simulations; H.F, J.Z, Y.D carried out STM

characterizations; H.F, L.R and J.C carried out electrochemical measurements. X.X, J.Z designed and carried out PPMS tests; C.L and J.W carried out the XPS measurements. H.F, S.X.D, Y.D and W.H wrote the manuscript. All authors contributed to data analysis, discussions and manuscript preparation.

Notes

The authors declare no competing financial interests.

REFERENCES

(1) Zeng, K.; Zhang, D. Recent Progress in Alkaline Water Electrolysis for Hydrogen Production and Applications. *Prog. Energy Combust. Sci.* **2010**, *36*, 307−326.

(2) Trotochaud, L.; Ranney, J. K.; Williams, K. N.; Boettcher, S. W. Solution-cast Metal Oxide Thin Film Electrocatalysts for Oxygen Evolution. *J. Am. Chem. Soc.* **2012**, *134*, 17253−17261.

(3) Louie, M. W.; Bell, A. T. An Investigation of Thin-film Ni–Fe Oxide Catalysts for the Electrochemical Evolution of Oxygen. *J. Am. Chem. Soc.* **2013**, *135*, 12329–12337.

(4) McCrory, C. C. L.; Jung, S.; Peters, J. C.; Jaramillo, T. F. Benchmarking Heterogeneous Electrocatalysts for the Oxygen Evolution Reaction. *J. Am. Chem. Soc.* **2013**, *135*, 16977−16987.

(5) Smith, R. D. L.; Prévot, M. S.; Fagan, R. D.; Trudel, S.; Berlinguette, C. P. Water Oxidation Catalysis: Electrocatalytic Response to Metal Stoichiometry in Amorphous Metal Oxide Films Containing Iron, Cobalt, and Nickel. *J. Am. Chem. Soc.* **2013**, *135*, 11580−11586.

(6) Zhang, B.; Zheng, X.; Voznyy, O.; Comin, R.; Bajdich, M.; García-Melchor, M.; Han, L.; Xu, J.; Liu, M.; Zheng, L.; Arquer, F. P. G. de; Dinh, C. T.; Fan, F.; Yuan, M.; Yassitepe, E.; Chen, N.; Regier, T.; Liu, P.; Li, Y.; Luna, P. D.; Janmohamed, A.; Xin, H. L.; Yang, H.; Vojvodic, A.; Sargent, E. H. Homogeneously Dispersed Multimetal Oxygen-evolving Catalysts. *Science* **2016**, *352*, 333−337.

(7) Meng, Y.; Song, W.; Huang, H.; Ren, Z.; Chen, S.-Y.; Suib, S. L. Structure-property Relationship of Bifunctional MnO_2 Nanostructures: Highly Efficient, Ultra-stable Electrochemical Water Oxidation and Oxygen Reduction Reaction Catalysts Identified in Alkaline Media. *J. Am. Chem. Soc.* **2014**, *136*, 11452–11464.

(8) Subbaraman, R.; Tripkovic, D.; Chang, K.-C.; Strmcnik, D.; Paulikas, A. P.; Hirunsit, P.; Chan, M.; Greeley, J.; Stamenkovic, V.; Markovic, N. M. Trends in Activity for the Water Electrolyser Reactions on 3d M(Ni,Co,Fe,Mn) Hydr(oxy)oxide Catalysts. *Nat. Mater.* **2012**, *11*, 550–557.

(9) Subbaraman, R.; Tripkovic, D.; Strmcnik, D.; Chang, K.-C.; Uchimura, M.; Paulikas, A. P.; Stamenkovic, V.; Markovic, N. M. Enhancing Hydrogen Evolution Activity in Water Splitting by Tailoring Li^+-$Ni(OH)_2$-Pt Interfaces. *Science* **2011**, *334*, 1256−1260.

(10) Stamenkovic, V. R.; Strmcnik, D.; Lopes, P. P.; Markovic, N. M. Energy and Fuels from Electrochemical Interfaces. *Nat. Mater.* **2017**, *16*, 57−69.

(11) Gong, M.; Zhou, W.; Tsai, M.-C.; Zhou, J.; Guan, M.; Lin, M.-C.; Zhang, B.; Hu, Y.; Wang, D.-Y.; Yang, J.; Pennycook, S. J.; Hwang, B.-J.; Dai, H. Nanoscale Nickel Oxide/Nickel Heterostructures for Active Hydrogen Evolution Electrocatalysis. *Nat. Commun.* **2014**, *5*, 4695.

(12) Feng, J.-X.; Xu, H.; Dong, Y.-T.; Lu, X.-F.; Tong, Y.-X.; Li, G.-R. Efficient Hydrogen Evolution Electrocatalysis Using Cobalt Nanotubes Decorated with Titanium Dioxide Nanodots. *Angew. Chem. Int. Ed.* **2017**, *129*, 3006–3010.

(13) Bates, M. K.; Jia, Q.; Ramaswamy, N.; Allen, R. J.; Mukerjee, S. Composite Ni/NiO-Cr_2O_3 Catalyst for Alkaline Hydrogen Evolution Reaction. *J. Phys. Chem. C* **2015**, *119*, 5467−5477.

(14) Zhu, Y. P.; Ma, T. Y.; Jaroniec, M.; Qiao, S. Z. Self-Templating Synthesis of Hollow Co_3O_4 Microtube Arrays for Highly Efficient Water Electrolysis. *Angew. Chem. Int. Ed.* **2017**, *56*, 1324–1328.

(15) Weng, Z.; Liu, W.; Yin, L.-C.; Fang, R.; Li, M.; Altman, E. I.; Fan, Q.; Li, F.; Cheng, H.-M.; Wang, H. Metal/Oxide Interface Nanostructures Generated by Surface Segregation for Electrocatalysis. *Nano Lett.* **2015**, *15*, 7704−7710.

(16) Gao, X.; Zhang, H.; Li, Q.; Yu, X.; Hong, Z.; Zhang, X.; Liang, C.; Lin, Z. Hierarchical $NiCo_2O_4$ Hollow Microcuboids as Bifunctional Electrocatalysts for Overall Water-Splitting. *Angew. Chem. Int. Ed.* **2016**, *55*, 6290–6294.

(17) Sun, M.; Chen, Y.; Tian, G.; Wu, A.; Yan, H.; Fu, H. Stable Mesoporous $ZnFe_2O_4$ as an Efficient Electrocatalyst for Hydrogen Evolution Reaction. *Electrochim. Acta* **2016**, *190*, 186−192.

(18) Venkatkarthick, R.; Davidson, D. J.; Ravichandran, S.; Vengatesan, S.; Sozhan, G.; Vasudevan, S. Eco-friendly and Facilely Prepared Silica Modified Amorphous Titania (TiO_2-SiO_2) Electrocatalyst for the O_2 and H_2 Evolution Reactions. *Catal. Sci. Technol.* **2015**, *5*, 5016−5022.

(19) Chanda, D.; Hnát, J.; Paidar, M.; Schauer, J.; Bouzek, K. Synthesis and Characterization of $NiFe_2O_4$ Electrocatalyst for the Hydrogen Evolution Reaction in Alkaline Water Electrolysis using Different Polymer Binders. *J. Power Sources* **2015**, *285*, 217−226.

(20) Wang, H.; Lee, H.-W.; Deng, Y.; Lu, Z.; Hsu, P.-C.; Liu, Y.; Lin, D.; Cui, Y. Bifunctional Non-noble Metal Oxide Nanoparticle Electrocatalysts through Lithium-induced Conversion for Overall Water Splitting. *Nat. Commun.* **2015**, *6*, 7261.

(21) Yan, X.; Tian, L.; He, M.; Chen, X. Three-Dimensional Crystalline/Amorphous Co/Co_3O_4 Core/Shell Nanosheets as Efficient Electrocatalysts for the Hydrogen Evolution Reaction. *Nano Lett.* **2015**, *15*, 6015−6021.

(22) Luo, Z.; Miao, R.; Huan, T. D.; Mosa, I. M.; Poyraz, A. S.; Zhong, W.; Cloud, J. E.; Kriz, D. A.; Thanneeru, S.; He, J.; Zhang, Y.; Ramprasad, R.; Suib, S. L. Mesoporous MoO_{3-x} Material as an Efficient Electrocatalyst for Hydrogen Evolution Reactions. *Adv. Energy Mater.* **2016**, *6*, 1600528.

(23) Jin, Y.; Wang, H.; Li, J.; Yue, X.; Han, Y.; Shen, P. K.; Cui, Y. Porous MoO_2 Nanosheets as Non-noble Bifunctional Electrocatalysts for Overall Water Splitting. *Adv. Mater.* **2016**, *28*, 3785–3790.

(24) Shu, C.; Kang, S.; Jin, Y.; Yue, X.; Shen, P. K. Bifunctional Porous Non-precious Metal WO_2 Hexahedral Networks as an Electrocatalyst for Full Water Splitting. *J. Mater. Chem. A* **2017**, *5*, 9655−9660.

(25) Yan, X.; Tian, L.; Atkins, S.; Liu, Y.; Murowchick, J.; Chen, X. Converting $CoMoO_4$ into CoO/MoO_x for Overall Water Splitting by Hydrogenation. *ACS Sustainable Chem. Eng.* **2016**, *4*, 3743−3749.

(26) Jin, Y.; Shen, P. K. Nanoflower-like Metallic Conductive MoO_2 as a High-performance Non-precious Metal Electrocatalyst for the Hydrogen Evolution Reaction. *J. Mater. Chem. A* **2015**, *3*, 20080−20085.

(27) Strmcnik, D.; Lopes, P. P.; Genorio, B.; Stamenkovic, V. R.; Markovic, N. M. Design Principles for Hydrogen Evolution Reaction Catalyst Materials. *Nano Energy* **2016**, *29*, 29−36.

(28) Seh, Z. W.; Kibsgaard, J.; Dickens, C. F.; Chorkendorff, I.; Nørskov, J. K.; Jaramillo, T. F. Combining Theory and Experiment in Electrocatalysis: Insights into Materials Design. *Science* *2017*, **355**, eaad4998.

(29) Ling, T.; Yan, D.-Y.; Wang, H.; Jiao, Y.; Hu, Z.; Zheng, Y.; Zheng, L.; Mao, J.; Liu, H.; Du, X.-W.; Jaroniec, M.; Qiao, S.-Z. Activating Cobalt(II) Oxide Nanorods for Efficient Electrocatalysis by Strain Engineering. *Nat. Commun.* **2017**, *8*, 1509.

(30) Diebold, U. The Surface Science of Titanium Dioxide. *Surf. Sci. Rep.* **2003**, *48*, 53−229.

(31) Stemmer, S.; Sane, A.; Browning, N. D.; Mazanec, T. J. Characterization of Oxygen-deficient $SrCoO_{3−\delta}$ by Electron Energy-loss Spectroscopy and Z-contrast Imaging. *Solid State Ionics* **2000**, *130*, 71−80.

(32) Setvin, M.; Franchini, C.; Hao, X.; Schmid, M.; Janotti, A.; Kaltak, M.; Walle, C. G. Van de; Kresse, G.; Diebold, U. Direct View at Excess Electrons in TiO_2 Rutile and Anatase. *Phys. Rev. Lett.* **2014**, *113*, 086402.

(33) Minato, T.; Sainoo, Y.; Kim, Y.; Kato, H. S.; Aika, K.-I.; Kawai, M.; Zhao, J.; Petek, H.; Huang, T.; He, W.; Wang, B.; Wang, Z.; Zhao, Y.; Yang, J.; Hou, J. G. The Electronic Structure of Oxygen Atom Vacancy and Hydroxyl Impurity Defects on Titanium Dioxide (110) Surface. *J. Chem. Phys.* **2009**, *130*,124502.

(34) Yim, C. M.; Watkins, M. B.; Wolf, M. J.; Pang, C. L.; Hermansson, K.; Thornton, G. Engineering Polarons at a Metal Oxide Surface. *Phys. Rev. Lett.* **2016**, *117*, 116402.

(35) Bikondoa, O.; Pang, C. L.; Ithnin, R.; Muryn, C. A.; Onishi, H.; Thornton, G. Direct Visualization of Defect-mediated Dissociation of Water on $TiO_2(110)$. *Nat. Mater.* **2006**, *5*, 189–192.

(36) Cui, X.; Wang, Z.; Tan, S.; Wang, B.; Yang, J.; Hou, J. G. Identifying Hydroxyls on the $TiO_2(110)$-1×1 Surface with Scanning Tunneling Microscopy. *J. Phys. Chem. C* **2009**, *113*, 13204–13208.
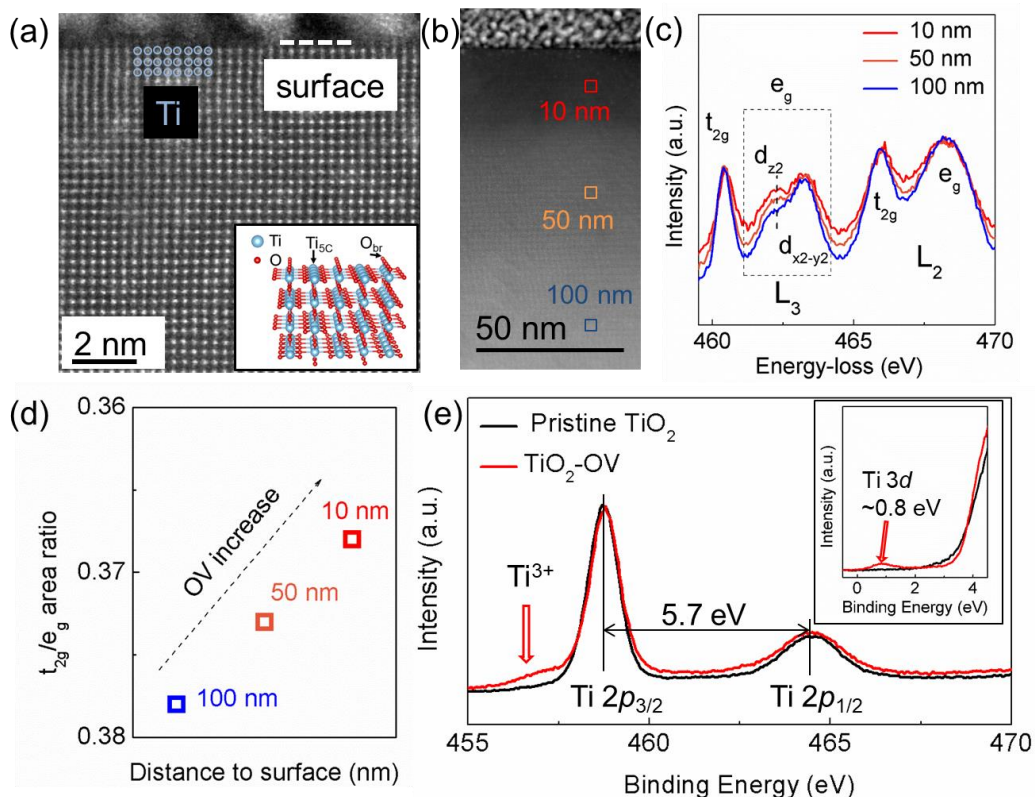
Figures and Figure captions.

Figure 1. (a) Cross-sectional scanning transmission electron microscopy (STEM) image of reduced $TiO_2(110)$ single crystal in HAADF mode, showing a high crystalline structure both in the surface and bulk regions. Inset is the crystal structure of the rutile $TiO_2(110)$. (b) Large-region cross-sectional STEM image of reduced $TiO_2(110)$ single crystal in HAADF mode, in which three areas with different depth from the surface (10 nm, 50 nm, and 100 nm) are marked. (c) Corresponding in-situ EELS Ti-*L* edge spectra of the three regions marked in (b). (d) Relative peak area ratio of the t_{2g} and e_g peaks acquired from (c), which indicates the gradually increasing OV concentration from the inner bulk region to the surface region. (e) In-situ Ti $2p$ XPS spectra of the pristine and reduced TiO_2 single crystal; inset shows valence band (VB) XPS spectra of pristine and reduced TiO_2 single crystal.
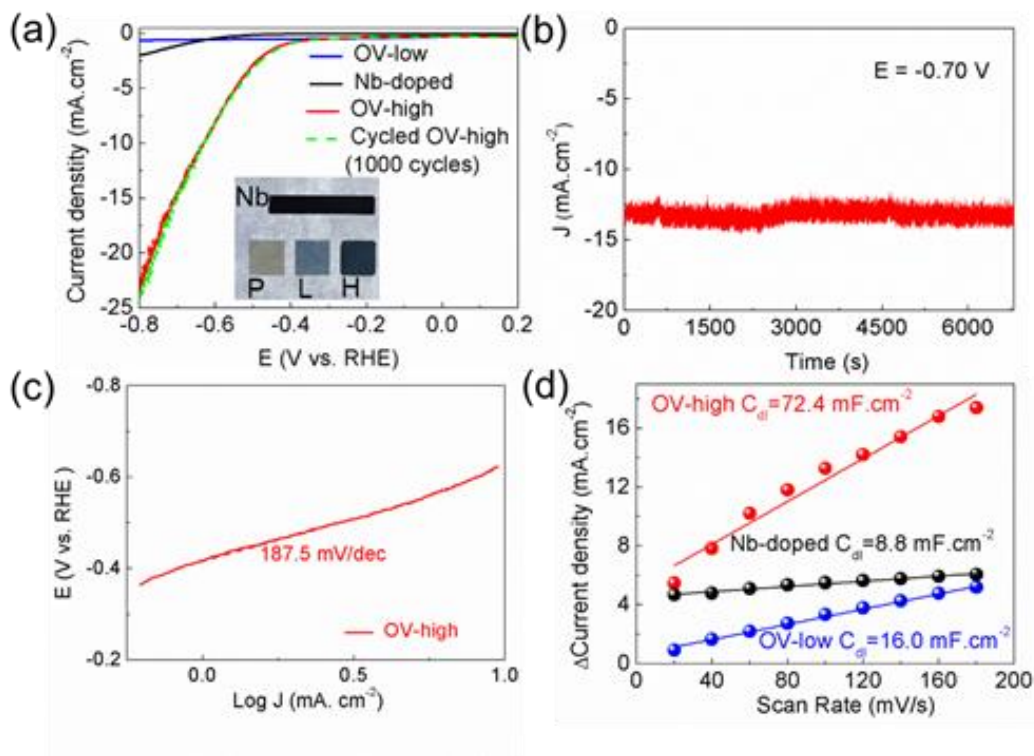
Figure 2. (a) Linear sweep voltammetric (LSV) data on different electrocatalysts for the HER at the rate of 10 mV·s^{-1}, inset shows the pristine $TiO_2(110)$ single crystal (P), OV-low $TiO_2(110)$ single crystal (L), OV-high $TiO_2(110)$ single crystal (H), and the Nb-doped $TiO_2(110)$ single crystal (Nb). The OV-high TiO_2 was tested for 1000 cycles with the LVS curve shown as the red solid and green dashed lines for before and after cycling, respectively. (b) Cycling stability over 18 h of the OV-high sample at a potential of –0.7 V. (c) Tafel plot of the OV-high TiO_2. (d) C_{dl} determined from the linear fitting of the capacitive current vs. scan rate, measured from the cyclic voltammetry (CV) curves of OV-high TiO_2, OV-low TiO_2 and Nb-doped TiO_2.
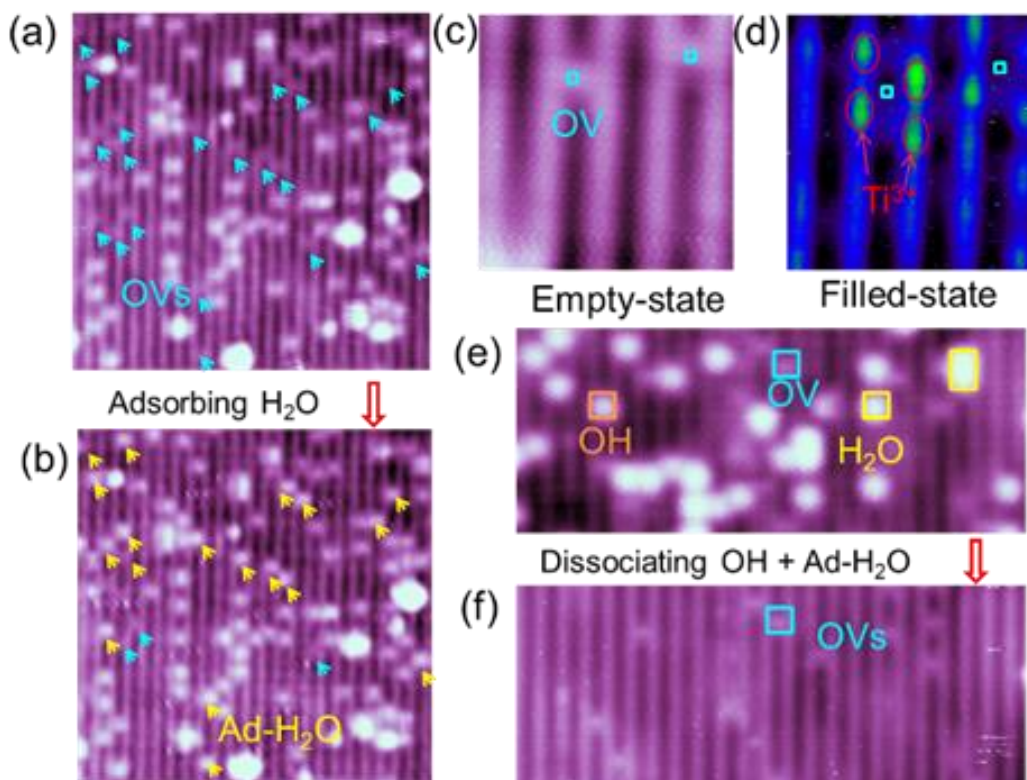
Figure 3. In-situ STM studies on electrocatalytic dynamics occurring on $TiO_2(110)$ surface associated with oxygen vacancies. (a) STM image of the partially hydroxylated TiO_2 surface, with the OVs indicated by light blue arrows (15 nm × 15 nm, 1.2 V, 20 pA). (b) STM image of the same region of a, with the OVs mostly filled by H_2O (15 nm × 15 nm, 1.2 V, 20 pA). (c) STM image of the reduced TiO_2 surface with two individual OVs in the empty-state (1.2 V, 20 pA). (d) STM image of the same region of (c), but in the filled-state, with Ti^{3+} ions indicated by red arrows (-2.3 V, 10 pA). (e) STM image of the partially hydroxylated TiO_2 surface, with OVs, OHs, and Ad-H_2O appearing on the surface (1.2 V, 20 pA). (f) STM image of the same region of e after the OHs and Ad-H_2O were removed by the last scan with a tip bias of 2.5 V. (1.2 V, 20 pA).
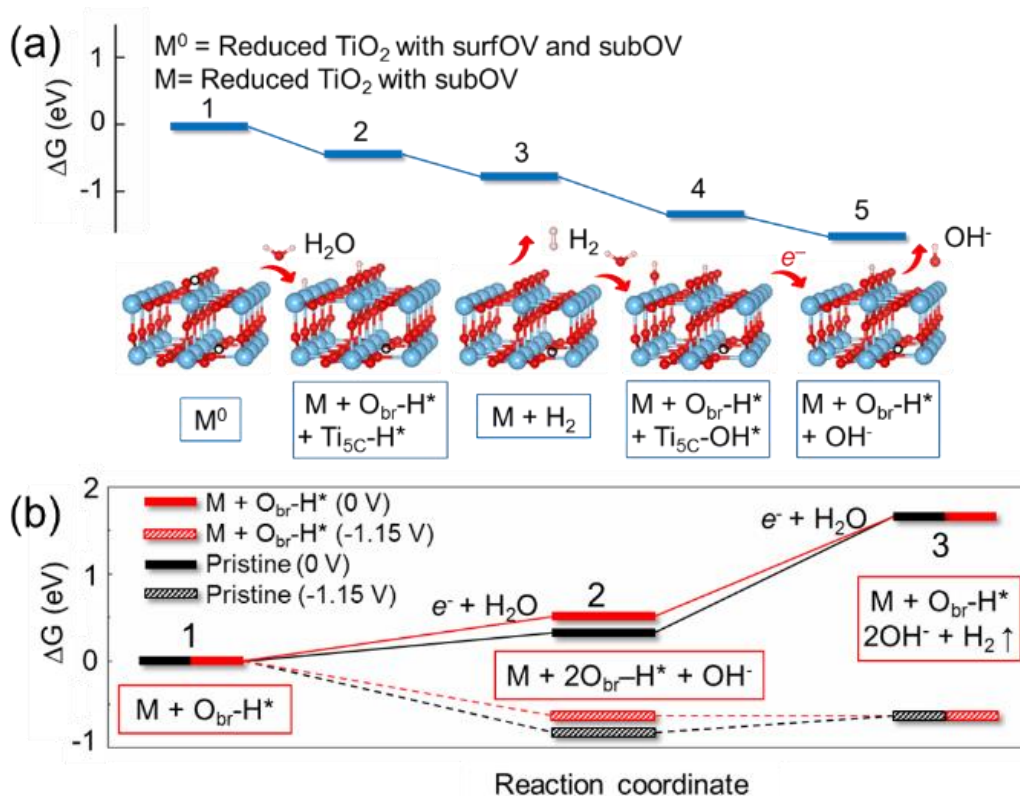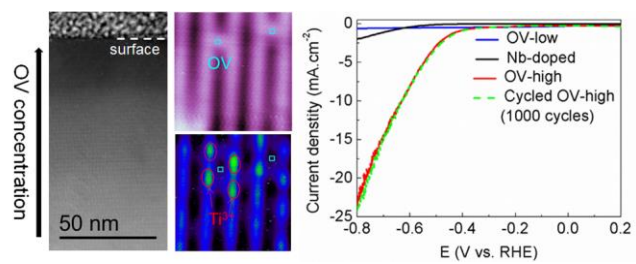
Figure 4. DFT calculations reveal roles of oxygen vacancies in electrocatalysis on $TiO_2(110)$ surface. (a) Free energy pathways of the relevant reaction intermediates in alkaline media on the reduced TiO_2 with both surfOV and subOV, with the OVs marked as solid black circles. (b) Compare of HER free energy of pristine TiO_2 and reduced TiO_2 with subOV and O_{br}-H^* (an onset potential of $U_{RHE} = -1.15$ V determined from the rate limiting step of electrocatalyst M was applied for both catalysts).

TOC